DISCOVERY OF GAMMA-RAY EMISSION FROM THE SHELL-TYPE SUPERNOVA REMNANT RCW 86 WITH HESS

F. AHARONIAN[1,2], A. G. AKHPERJANIAN[3], U. BARRES DE ALMEIDA[4,31], A. R. BAZER-BACHI[5], B. BEHERA[6], M. BEILICKE[7], W. BENBOW[1], K. BERNLÖHR[1,8], C. BOISSON[9], A. BOCHOW[1], V. BORREL[5], I. BRAUN[1], E. BRION[10], J. BRUCKER[11], R. BÜHLER[1], T. BULIK[12], I. BÜSCHING[13], T. BOUTELIER[14], S. CARRIGAN[1], P. M. CHADWICK[4], A. CHARBONNIER[15], R. C. G. CHAVES[1], L.-M. CHOUNET[16], A. C. CLAPSON[1], G. COIGNET[17], L. COSTAMANTE[1,32], M. DALTON[8], B. DEGRANGE[16], H. J. DICKINSON[4], A. DJANNATI-ATAÏ[18], W. DOMAINKO[1], L.O'C. DRURY[2], F. DUBOIS[17], G. DUBUS[14], J. DYKS[12], K. EGBERTS[1], D. EMMANOULOPOULOS[6], P. ESPIGAT[18], C. FARNIER[19], F. FEINSTEIN[19], A. FIASSON[19], A. FÖRSTER[1], G. FONTAINE[16], M. FÜSSLING[8], S. GABICI[2], Y. A. GALLANT[19], L. GÉRARD[18], B. GIEBELS[16], J. F. GLICENSTEIN[10], B. GLÜCK[11], P. GORET[10], C. HADJICHRISTIDIS[4], D. HAUSER[6], M. HAUSER[6], G. HEINZELMANN[7], G. HENRI[14], G. HERMANN[1], J. A. HINTON[20], A. HOFFMANN[21], W. HOFMANN[1], M. HOLLERAN[13], S. HOPPE[1,33], D. HORNS[7], A. JACHOLKOWSKA[15], O. C. DE JAGER[13], I. JUNG[11], K. KATARZYŃSKI[22], S. KAUFMANN[6], E. KENDZIORRA[21], M. KERSCHHAGGL[8], D. KHANGULYAN[1], B. KHÉLIFI[16], D. KEOGH[4], Nu. KOMIN[19], K. KOSACK[1], G. LAMANNA[17], I. J. LATHAM[4], M. LEMOINE-GOUMARD[23,33], J.-P. LENAIN[9], T. LOHSE[8], V. MARANDON[18], J. M. MARTIN[9], O. MARTINEAU-HUYNH[15], A. MARCOWITH[19], C. MASTERSON[2], D. MAURIN[15], T. J. L. McCOMB[4], C. MEDINA[9], R. MODERSKI[12], E. MOULIN[10], M. NAUMANN-GODO[16], M. DE NAUROIS[15], D. NEDBAL[24], D. NEKRASSOV[1], J. NIEMIEC[25], S. J. NOLAN[4], S. OHM[1], J-F. OLIVE[5], E. DE OÑA WILHELMI[32], K. J. ORFORD[4], J. L. OSBORNE[4], M. OSTROWSKI[26], M. PANTER[1], G. PEDALETTI[6], G. PELLETIER[14], P.-O. PETRUCCI[14], S. PITA[18], G. PÜHLHOFER[6], M. PUNCH[18], A. QUIRRENBACH[6], B. C. RAUBENHEIMER[13], M. RAUE[1,32], S. M. RAYNER[4], M. RENAUD[1], F. RIEGER[1,32], J. RIPKEN[7], L. ROB[24], S. ROSIER-LEES[17], G. ROWELL[27], B. RUDAK[12], J. RUPPEL[28], V. SAHAKIAN[3], A. SANTANGELO[21], R. SCHLICKEISER[28], F. M. SCHÖCK[11], R. SCHRÖDER[28], U. SCHWANKE[8], S. SCHWARZBURG[21], S. SCHWEMMER[6], A. SHALCHI[28], J. L. SKILTON[20], H. SOL[9], D. SPANGLER[4], Ł. STAWARZ[26], R. STEENKAMP[29], C. STEGMANN[11], G. SUPERINA[16], P. H. TAM[6], J.-P. TAVERNET[15], R. TERRIER[18], O. TIBOLLA[6], C. VAN ELDIK[1], G. VASILEIADIS[19], C. VENTER[13], J. P. VIALLE[17], P. VINCENT[15], J. VINK[30], M. VIVIER[10], H. J. VÖLK[1], F. VOLPE[16,32], S. J. WAGNER[6], M. WARD[4], A. A. ZDZIARSKI[12], AND A. ZECH[9]

[1] Max-Planck-Institut für Kernphysik, P.O. Box 103980, D 69029 Heidelberg, Germany
[2] Dublin Institute for Advanced Studies, 5 Merrion Square, Dublin 2, Ireland
[3] Yerevan Physics Institute, 2 Alikhanian Brothers St., 375036 Yerevan, Armenia
[4] Department of Physics, University of Durham, South Road, Durham DH1 3LE, UK
[5] Centre d'Etude Spatiale des Rayonnements, CNRS/UPS, 9 av. du Colonel Roche, BP 4346, F-31029 Toulouse Cedex 4, France
[6] Landessternwarte, Universität Heidelberg, Königstuhl, D 69117 Heidelberg, Germany
[7] Universität Hamburg, Institut für Experimentalphysik, Luruper Chaussee 149, D 22761 Hamburg, Germany
[8] Institut für Physik, Humboldt-Universität zu Berlin, Newtonstr. 15, D 12489 Berlin, Germany
[9] LUTH, Observatoire de Paris, CNRS, Université Paris Diderot, 5 Place Jules Janssen, 92190 Meudon, France
[10] IRFU/DSM/CEA, CE Saclay, F-91191 Gif-sur-Yvette, Cedex, France
[11] Universität Erlangen-Nürnberg, Physikalisches Institut, Erwin-Rommel-Str. 1, D 91058 Erlangen, Germany
[12] Nicolaus Copernicus Astronomical Center, ul. Bartycka 18, 00-716 Warsaw, Poland
[13] Unit for Space Physics, North-West University, Potchefstroom 2520, South Africa
[14] Laboratoire d'Astrophysique de Grenoble, INSU/CNRS, Université Joseph Fourier, BP 53, F-38041 Grenoble Cedex 9, France
[15] LPNHE, Université Pierre et Marie Curie Paris 6, Université Denis Diderot Paris 7, CNRS/IN2P3, 4 Place Jussieu, F-75252, Paris Cedex 5, France
[16] Laboratoire Leprince-Ringuet, Ecole Polytechnique, CNRS/IN2P3, F-91128 Palaiseau, France
[17] Laboratoire d'Annecy-le-Vieux de Physique des Particules, CNRS/IN2P3, 9 Chemin de Bellevue, BP 110 F-74941 Annecy-le-Vieux Cedex, France
[18] Astroparticule et Cosmologie (APC), CNRS, Universite Paris 7 Denis Diderot, 10, rue Alice Domon et Leonie Duquet, F-75205 Paris Cedex 13, France
[19] Laboratoire de Physique Théorique et Astroparticules, CNRS/IN2P3, Université Montpellier II, CC 70, Place Eugène Bataillon, F-34095 Montpellier Cedex 5, France
[20] School of Physics & Astronomy, University of Leeds, Leeds LS2 9JT, UK
[21] Institut für Astronomie und Astrophysik, Universität Tübingen, Sand 1, D 72076 Tübingen, Germany
[22] Toruń Centre for Astronomy, Nicolaus Copernicus University, ul. Gagarina 11, 87-100 Toruń, Poland
[23] Université Bordeaux I, CNRS/IN2P3, Centre d'Etudes Nucléaires de Bordeaux Gradignan, UMR 5797, Chemin du Solarium, 33175 Gradignan, France; lemoine@cenbg.in2p3.fr
[24] Institute of Particle and Nuclear Physics, Charles University, V Holesovickach 2, 180 00 Prague 8, Czech Republic
[25] Instytut Fizyki Jądrowej PAN, ul. Radzikowskiego 152, 31-342 Kraków, Poland
[26] Obserwatorium Astronomiczne, Uniwersytet Jagielloński, Kraków, Poland
[27] School of Chemistry & Physics, University of Adelaide, Adelaide 5005, Australia
[28] Institut für Theoretische Physik, Lehrstuhl IV: Weltraum und Astrophysik, Ruhr-Universität Bochum, D 44780 Bochum, Germany
[29] University of Namibia, Private Bag 13301, Windhoek, Namibia
[30] Astronomical Institute, Utrecht University, P.O. Box 80000, 3508 TA Utrecht, The Netherlands

ABSTRACT

The shell-type supernova remnant (SNR) RCW 86, possibly associated with the historical supernova SN 185, with its relatively large size (about $40'$ in diameter) and the presence of nonthermal X-rays is a promising target for γ-ray observations. The high sensitivity, good angular resolution of a few arcminutes and the large field of view of the High Energy Stereoscopic System (HESS) make it ideally suited for the study of γ-ray morphology of such extended sources. HESS observations have indeed led to the discovery of the SNR RCW 86 in very high energy (VHE; $E > 100$ GeV) γ-rays. With 31 hr of observation time, the source is detected with a statistical significance

of 8.5σ and is significantly more extended than the HESS point-spread function. Morphological studies have been performed and show that the γ-ray flux does not correlate perfectly with the X-ray emission. The flux from the remnant is $\sim 10\%$ of the flux from the Crab nebula, with a similar photon index of about 2.5. Possible origins of the VHE γ-ray emission, via either Inverse Compton scattering by electrons or the decay of neutral pions produced by proton interactions, are discussed on the basis of spectral features obtained both in the X-ray and γ-ray regimes.

Key words: gamma rays: observations – ISM: individual (RCW 86, G315.4-2.3) – supernova remnants

1. INTRODUCTION

Shell-type supernova remnants (SNRs) are widely believed to be the prime candidates for accelerating cosmic ray protons and nuclei up to 10^{15} eV. A promising way of proving the existence of high-energy hadrons accelerated in SNR shells is the detection of very high energy (VHE; $E > 100$ GeV) γ-rays produced in nucleonic interactions with ambient matter. VHE γ-ray emission has been detected recently in several shell-type SNRs, especially from Cassiopeia A (Aharonian et al. 2001; Albert et al. 2007), RX J1713.7−3946 (Aharonian et al. 2007a), and RX J0852.0−4622 (Aharonian et al. 2007b). These two latest sources both show an extended morphology highly correlated with the structures seen in nonthermal X-rays. Although a hadronic origin is probable in the above cases (e.g., Berezhko & Völk 2006), a leptonic origin cannot be ruled out (e.g., Porter et al. 2006).

Another young shell-type SNR is RCW 86 (also known as G315.4−2.3 and MSH 14−63). It has a complete shell in radio (Kesteven & Caswell 1987), optical (Smith 1997), and X-rays (Pisarski et al. 1984), with a nearly circular shape of $40'$ diameter. It received substantial attention because of its possible association with SN 185, the first historical Galactic supernova (SN; Clark & Stephenson 1977). However, conclusive evidence for this connection is still missing: using optical observations, Rosado et al. (1996) found an apparent kinematic distance of 2.8 kpc and an age of $\sim 10,000$ years, whereas recent observations of the northeast part of the remnant with the *Chandra* and *XMM-Newton* satellites strengthen the case that the event recorded by the Chinese in 185 AD was a supernova and that RCW 86 is its remnant (Vink et al. 2006). In this case, a distance to the SNR of ~ 1 kpc can be estimated for a standard Sedov evolution scenario (Bocchino et al. 2000). The X-ray spectrum obtained with the *Einstein* satellite was first represented by a two-temperature plasma model (Winkler 1978). Then, *Rossi X-Ray Timing Explorer* (*RXTE*; Petre et al. 1999) and *ASCA* observations (Bamba et al. 2000; Borkowski et al. 2001), with a wider spectral coverage, were used to resolve a nonthermal component in the X-ray spectrum which can be well described by a soft power law with a photon index of ~ 3. The large-scale density gradient across RCW 86 (Pisarski et al. 1984; Claas et al. 1989) possibly suggests that the northern part could be the shocked half of a very low density wind bubble plus dense shell from the progenitor star, and to this extent it could well be similar to RX J1713.7−3946 and RX J0852.0−4622. In its southern part, RCW 86 contains an H II region. Apparently, the gas density in this H II region is rather high and spatially extended. Therefore, the SNR shock has swept over an extended high-density region in the South, with consequent high radio

and thermal X-ray emissions (Bocchino et al. 2000). With a diameter of about $40'$, RCW 86 is one of the very few nonthermal X-ray-emitting SNRs resolvable in VHE γ-rays. High Energy Stereoscopic System (HESS), with its high sensitivity, its good angular resolution, and its large field of view is ideally suited for morphology studies of such an extended object.

Evidence for γ-ray emission from RCW 86 was found using the CANGAROO-II instrument, but no firm detection was claimed (Watanabe et al. 2003). Here, we present data on RCW 86 obtained with the full HESS array between 2004 and 2007.

2. HESS OBSERVATIONS AND ANALYSIS METHODS

HESS is an array of four imaging Cherenkov telescopes located 1800 m above sea level in the Khomas Highland in Namibia (Hinton 2004). Each telescope has a tesselated mirror with an area of 107 m^2 (Bernlöhr et al. 2003) and is equipped with a camera comprising of 960 photomultipliers (Vincent et al. 2003) covering a field of view of $5°$ in diameter. Due to the effective rejection of hadronic air showers with the stereoscopic imaging technique, the HESS telescope system can detect point sources near zenith at flux levels of about 1% of the Crab nebula flux with a statistical significance of 5σ standard deviation in 25 hr of observation (Aharonian et al. 2006).

The shell-type SNR RCW 86 was observed between 2004 and 2007 with the complete HESS array. After standard data quality selection and dead time correction, the resulting live time is 31 hr. The observations have been carried out at zenith angles ranging from $38°$ to $53°$. The data were taken using the wobble mode where the source is offset from the center of the field of view, alternating between 28 minute runs in the positive and negative declination or right ascension directions; the mean offset angle of the data set used in this analysis is $0°.7$. The energy threshold of the system increases with zenith angle: for the observations presented here, the average threshold was 480 GeV.

The data were calibrated using standard HESS calibration procedures, as discussed by Aharonian et al. (2004). The data were analyzed using a Hillas-parameter-based method as described in Aharonian et al. (2005) with *standard* cuts, which include a minimum requirement of 80 photoelectrons in each camera image. Two different background estimation procedures were used, as described in Berge et al. (2007). For two-dimensional image generation and morphology studies, the *ring background* method was applied with a mean ring radius of $0°.7$. As this method uses an energy-averaged radial acceptance correction, the *reflected-region background* method was applied for spectral studies. In this second background-subtraction procedure, OFF events were selected from the same field of view and in the same runs as the ON events by selecting the region symmetric to the ON region with respect to the camera center. As a cross-check, a second analysis chain, sharing only the raw data and using the "Combined Model" analysis
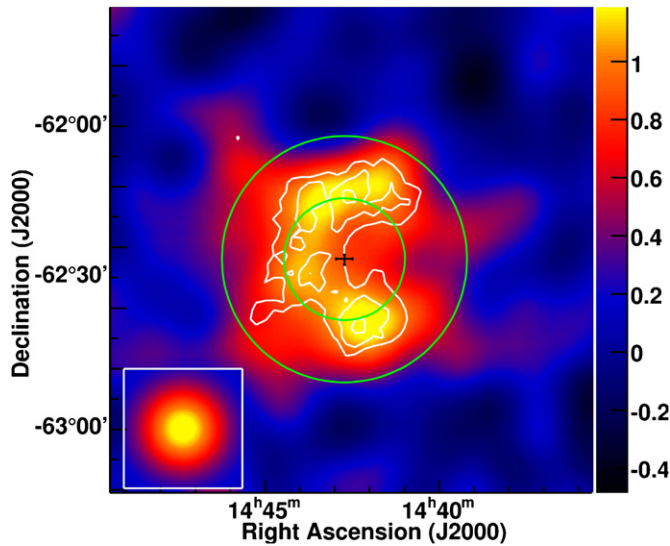
Figure 1. HESS γ-ray image of RCW 86. The map was smoothed with a Gaussian function with a $\sigma_{smooth} = 4'.8$ to reduce the effect of statistical fluctuations. The linear color scale is in units of excess counts per arcmin². White contours correspond to 4σ, 5σ, 6σ significance, obtained by counting gamma rays within $0'.14$ from each given location. The image inset in the bottom left corner indicates the size of a point source as seen by HESS, for an equivalent analysis, smoothing and zenith angles. The center of the fitted shell, as discussed in the text, is marked by a black cross. The two solid green circles correspond to the inner and outer radii of this shell.

(de Naurois et al. 2005), was also applied to the data. The two analysis methods yield consistent results.

3. RESULTS

A clear VHE γ-ray signal of 8.5σ standard deviation and 1546 ± 183 excess γ-rays is detected from a circular region of $0'.45$ radius, centered on ($\alpha_{J2000} = 14^h42^m43^s$, $\delta_{J2000} = -62°28'48''$). This integration region was chosen a priori on the basis of the X-ray data obtained with the *ROSAT* satellite and fully encompasses the SNR. Figure 1 shows the VHE γ-ray excess map of the $1°.6 \times 1°.6$ region around RCW 86. The map has been smoothed with a Gaussian kernel with a σ of $4'.8$ to suppress statistical fluctuations on scales smaller than the HESS point-spread function (PSF). The VHE γ-ray excess from RCW 86 is significantly extended beyond the PSF of the instrument, which is illustrated in the bottom-left corner of Figure 1. Contours of constant significance are superimposed in white at the 4σ, 5σ, and 6σ levels. An excess map has also been produced with the so-called "hard cuts" for better gamma hadron separation, which includes a stricter cut of 200 photoelectrons on the image size compared to the "standard cuts," and was found to be compatible with Figure 1. The VHE emission shown in Figure 1 is suggestive of a shell-like morphology. To test this hypothesis, the brightness profile of a thick shell projected along the line of sight and folded with the HESS PSF was fitted to the unsmoothed excess map. As illustrated in Figure 1, the best fit ($\chi^2/ndf = 233.1/220$) is obtained with an outer radius of $24'.43 \pm 1'.79_{stat}$, a width of $12'.39 \pm 4'.22_{stat}$, and a center of the shell at ($\alpha_{J2000} = 14^h42^m42.96^s \pm 14.1^s_{stat}$, $\delta_{J2000} = -62°26'41''.6 \pm 66''.5_{stat}$). Figure 2 shows the radial profile of the VHE excess relative to the fitted center. The fit of the radial profiles to the data points results in a chi-square per degree of freedom of $\chi^2/ndf = 2.85/7$ for a projected shell (determined by outer ring radius, ring width, and absolute normalization) which is not significantly better than the fit of a projected uniformly emitting sphere characterized by
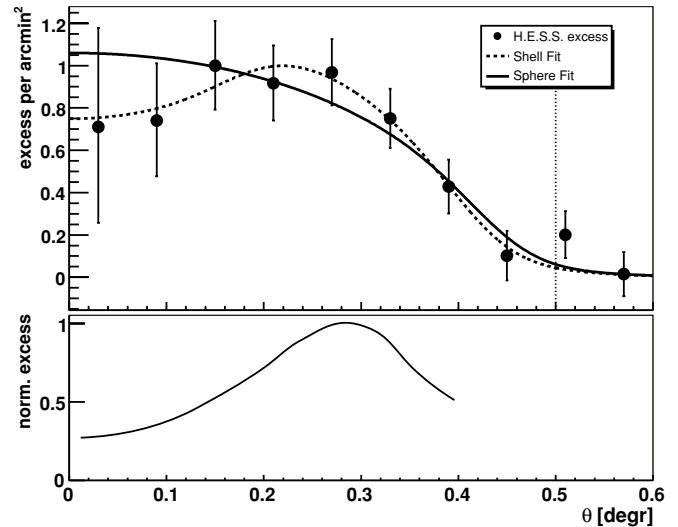

Figure 2. Upper panel: HESS radial profiles around the fitted center of the SNR ($\alpha_{J2000} = 14^h42^m43^s$, $\delta_{J2000} = -62°26'42''$). The solid line shows the result of a projected uniformly emitting sphere smoothed with the HESS PSF and fitted to the HESS data. The dashed line corresponds to a projection of a thick and spherically symmetric shell. The dotted vertical line illustrates the extent of the region used for the azimuthal profile and for the spectral analysis. Lower panel: radial profiles of the X-ray data (3–6 keV) from *XMM-Newton*. These data are background subtracted and smoothed to match the HESS angular resolution. Additionally, the obtained excess profile was normalized.
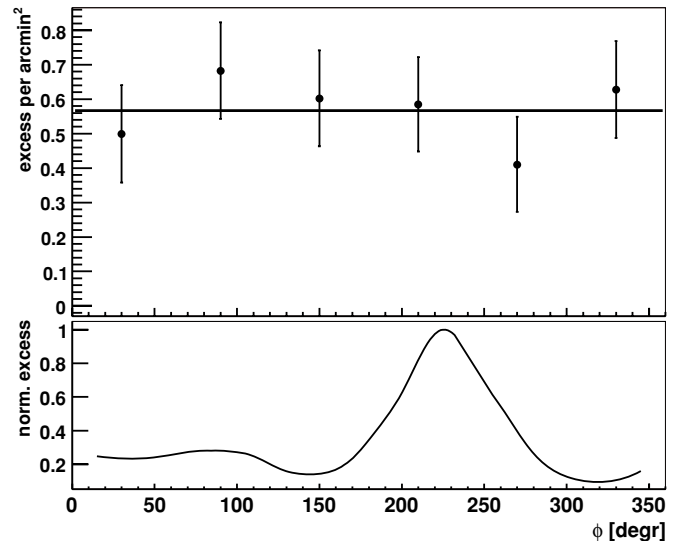
Figure 3. Upper panel: HESS azimuthal profile integrated over a region of $0°.5$ radius covering the SNR RCW 86. The azimuthal angle is calculated with respect to the fitted shell center. $0°$ corresponds to the north part of the source and $90°$ to the east. The solid line shows the result of a fit of the data to a constant which yields a chi-square of 1.47 for 5 degrees of freedom. Lower panel: azimuthal profiles of the X-ray data (3–6 keV) from *XMM-Newton*. These data are background subtracted and smoothed to match the HESS angular resolution. Additionally, the obtained excess profile was normalized.

a ring radius and a normalization factor ($\chi^2/ndf = 5.43/8$). Also visible in Figure 1 is an apparent deficit of γ-rays at the western part of the SNR. However, the azimuthal profile in Figure 3 is consistent with a constant and reveals that this dip is not significant ($\chi^2/ndf = 1.47/5$).
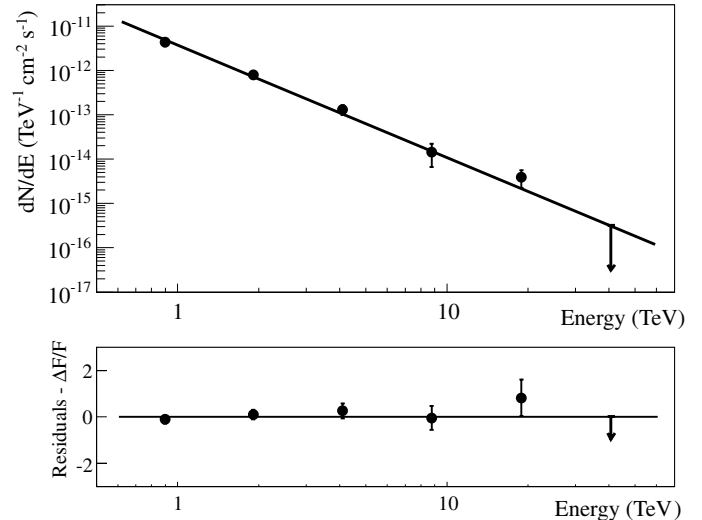
Figure 4 shows the 3–6 keV X-ray map of RCW 86 obtained using six observations of the remnant carried out by the *XMM-Newton* satellite in 2006 (Vink et al. 2006) and additional observations taken in 2007. The energy range was selected to
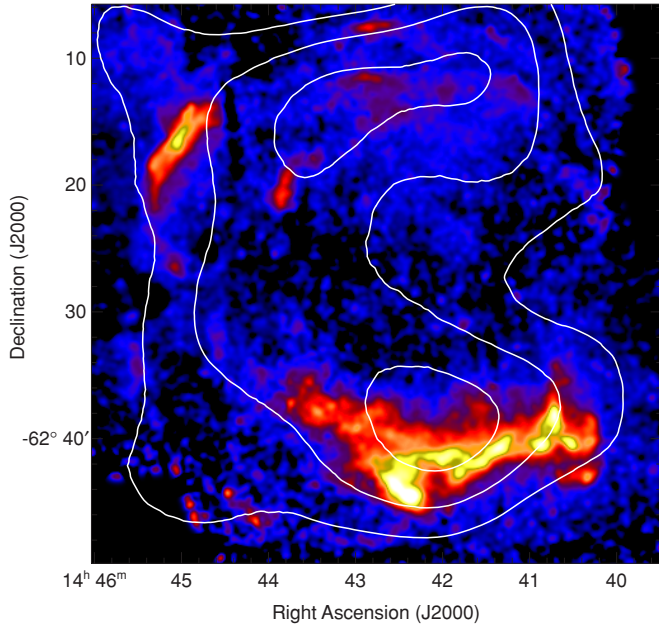
Figure 4. Excess contours of γ-ray emission (0.55, 0.8, and 1.05 γ-rays per arcmin^2 Gaussian smoothed with $\sigma_{smooth} = 4.8$) superimposed on the background-subtracted *XMM-Newton* EPIC (MOS/PN) 3–6 keV X-ray image of the remnant.

Figure 5. Differential energy spectrum of RCW 86, extracted from a circular region of 0.5 radius around the position ($\alpha_{J2000} = 14^h42^m43^s$, $\delta_{J2000} = -62°26'42''$) adjusted to the HESS data to enclose the whole source. The solid line shows the result of a pure power-law fit. The error bars denote 1σ statistical errors; the upper limit (arrow) is estimated at the 2σ level. The bottom panel shows the residuals to the power-law fit. Events with energies between 600 GeV and 60 TeV were used in the determination of the spectrum.

avoid as much as possible contamination from line emission from the, in general, cool plasma (< 1 keV) of RCW 86. Potentially, the 3–4 keV range could contain some contamination from Ar and Ca lines, but no such line emission is seen in the available *Chandra, XMM-Newton* (Vink et al. 2006) or *Suzaku* spectra (Ueno et al. 2007). This map was obtained by first automatically cleaning the observations of $> 3\sigma$ excursions to the mean count rate, thus minimizing the background of the maps. Then, for each observation and for each of the three detectors (MOS1, MOS2, and PN), a background count rate in the 3–6 keV band was determined using a relatively empty region of the field of view. In the final stage, the background image was subtracted from the count rate image, and then corrected using the exposure maps obtained with the standard *XMM-Newton* SAS 7.1.0 software (which includes vignetting correction), in order to obtain the background corrected map displayed in Figure 4. An overall positional agreement with the HESS contours derived from Figure 1 as well as a good compatibility between the outer radius of the γ-ray emission ($24.43 \pm 1.79_{stat}$) and the extension of the X-ray emission can be observed. However, the emission peak apparent in the X-ray azimuthal profile is not visible in γ-rays (Figure 3). Furthermore, the dip in surface brightness at the center of the remnant seems more pronounced in the X-ray radial profiles (Figure 2). A more detailed comparison of the γ-ray and X-ray morphologies would require higher statistics than presently available, and hence will have to await future longer observations.

For the spectral analysis, the source region (ON region) is defined by a circle of 0.5 radius centered on the best-fit position of the shell, chosen to fully enclose the whole source. The radius of the extraction region is illustrated in Figure 2. The spectrum obtained (see Figure 5) is well described by a power law with a photon index of $2.54 \pm 0.12_{stat} \pm 0.20_{sys}$ and a flux normalization at 1 TeV of $(3.72 \pm 0.50_{stat} \pm 0.8_{sys}) \times 10^{-12} cm^{-2}s^{-1}TeV^{-1}$ ($\chi^2/ndf = 6.30/4$). The integral flux in the energy range 1–10 TeV is $(2.34 \pm 0.3_{stat} \pm 0.5_{sys}) \times$

10^{-12} cm^{-2}s^{-1}, which corresponds to $\sim 10\%$ of the integrated flux of the Crab nebula in the same energy interval. No significant improvement is obtained by fitting a power law with an exponential cutoff ($\chi^2/ndf = 2.96/3$). If the fit range is restricted to energies below 10 TeV, a photon index of $2.41 \pm 0.16_{stat} \pm 0.20_{sys}$ and a flux normalization at 1 TeV of $(3.57 \pm 0.5_{stat} \pm 0.8_{sys}) \times 10^{-12}$ cm^{-2} s^{-1} TeV^{-1} are determined ($\chi^2/ndf = 0.68/2$), compatible with the fit of the SNR in the whole energy range.

4. DISCUSSION

There are two commonly invoked mechanisms for VHE γ-ray production in young SNRs, inverse Compton (IC) scattering of high-energy electrons off ambient photons (leptonic scenario) and π^0 meson production in inelastic interactions of accelerated protons with ambient gas (hadronic scenario). In such a hadronic scenario, a comparison between the expected thermal X-ray emission and the actual measured thermal emission has to await deeper observations in which one can better determine whether the TeV emission traces the denser, thermal X-ray-emitting parts of the SNR, or is more closely correlated with the X-ray synchrotron emission from the remnant.

The measured γ-ray spectrum from RCW 86, restricted to energies below 10 TeV, translates into an energy flux between 1 and 10 TeV of 8.6×10^{-12} erg cm^{-2} s^{-1}. The X-ray spectrum of the whole remnant is mixed between thermal and nonthermal emissions. Assuming that the hard X-ray continuum originates from nonthermal synchrotron emission as reported by Rho et al. (2002), Vink et al. (2006), and Ueno et al. (2007), the measurement made by Petre et al. (1999) using *RXTE* data provides an estimate of the total amount of nonthermal flux from RCW 86. They find that the spectrum is well fitted by a power law of index ~ 3 and a flux normalization at 10 keV of 10^{-4} cm^{-2} s^{-1} keV^{-1}, which extrapolated down to the 0.7–10 keV band leads to an integral flux of 2.1×10^{-10} erg cm^{-2} s^{-1}. In a leptonic scenario, assuming that the γ-ray emission is entirely due to the IC process on cosmic

microwave background photons, the ratio of the synchrotron power and IC power radiated is often used to constrain the magnetic field. For a power-law distribution of electron energies, $K\gamma^{-p}$, the general equation relating the synchrotron power (P_S) produced by electrons with Lorentz factors between $\gamma_{1,X}$ and $\gamma_{2,X}$ and the IC power ($P_{\rm IC}$) radiated between $\gamma_{1,IC}$ and $\gamma_{2,IC}$ can be expressed as follows:

$$\frac{P_S}{P_{\rm IC}} = \frac{U_B}{U_{ph}} \frac{\left(\gamma_{2,X}^{3-p} - \gamma_{1,X}^{3-p}\right)}{\left(\gamma_{2,\rm IC}^{3-p} - \gamma_{1,\rm IC}^{3-p}\right)} \qquad (1)$$

where $U_{\rm ph}$ and U_B are the energy density of the photon field and the energy density of the magnetic field, respectively. It should be noted here that, for a fixed X-ray energy, $\gamma_{1,X}$ and $\gamma_{2,X}$ are inversely proportional to the square root of the magnetic field. If X-rays and γ-rays probe the same region of the electron spectrum, one finds the standard relation between the synchrotron and IC power $\frac{P_S}{P_{\rm IC}} = \frac{U_B}{U_{\rm ph}}$. Assuming that the target photon field is the cosmic microwave background, a magnetic field of 30 μG can be estimated using Equation (1) and the synchrotron photon index of $\sim$3, independent of the distance and age of the SNR. This estimate is compatible with that of Vink et al. (2006) based on thin filaments resolved by *Chandra* (assuming a distance of 2.5 kpc) in which the authors also deduce a high speed of the blast wave ($\sim$ 2700 km s^{-1}); their estimated value would increase to $\sim$ 50 μG for a distance of 1 kpc. However, it is still a factor of 2 lower than the maximum field strength determined by Völk et al. (2005) using a lower shock velocity of 800 km s^{-1} as suggested by optical data in the Southern region of the SNR (Rosado et al. 1996). The difference between the field amplification estimated by Vink et al. (2006) and that of Völk et al. (2005) lies in the fact that Völk et al. obtained a higher result when they deprojected the measured filament width, as for an ideal spherical shock, whereas Vink et al. did not. Without deprojection the two results remarkably agree, even though they were obtained for the southern side and the northern side, respectively. A discussion of deprojection for RCW 86 is given in Völk et al. (2005). With similar data, Bamba et al. (2005) deduced a significantly lower magnetic field strength of $\sim$ 4–12 μG. However, their analysis is based on rather different assumptions on the nature of filament formation.

In a hadronic scenario, one can estimate the total energy in accelerated protons W_p in the range 10–100 TeV required to produce the γ-ray luminosity L_γ observed by HESS using the relation $W_p(10\text{–}100\text{ TeV}) \approx \tau_\gamma \times L_\gamma(1\text{–}10\text{ TeV})$, in which $\tau_\gamma \approx 4.9 \times 10^{15} \left(\frac{n}{1\,{\rm cm}^{-3}}\right)^{-1}$ s is the characteristic cooling time of protons through the π^0 production channel (Kelner et al. 2006). The total energy injected in protons is calculated by extrapolating the proton spectrum down to 1 GeV. Because of this extrapolation over four decades in energy, the uncertainty of the estimate can be as large as a factor of 10. Assuming that the relatively steep slope of the proton spectrum (as inferred from the observed γ-ray spectrum) is the result of an energy cutoff (somewhere around several tens of TeV in proton energy), and that at lower energies the proton spectrum has a E^{-2} type spectrum representative of those predicted by the diffusive shock acceleration theory, the total energy budget in all protons for the distance of 2.5 kpc and the ambient gas density between 0.3 cm^{-3} and 0.7 cm^{-3} (Bocchino et al. 2000), would be $(2\text{–}4) \times 10^{50}$ erg. This estimate is in reasonable agreement with theoretical expectations that a significant fraction of the explosion energy of 10^{51} erg is released in relativistic protons.

On the other hand, if the power-law spectrum of protons continues to GeV energies with the spectral index $\Gamma = 2.4$ (i.e., similar to the γ-ray spectrum below 10 TeV), the total budget in protons would exceed a few times 10^{51} erg for a distance of 2.5 kpc. This would exclude the hadronic origin of TeV γ-rays, unless the SNR is nearby ($\sim$ 1 kpc), or the γ-rays are produced in very dense regions. Indeed, Pisarski et al. (1984) and Claas et al. (1989) reported that there is a large density contrast across the remnant, e.g., in the South, where the density could be as high as 10 cm^{-3}; with such a dense medium, a larger distance for the remnant could still be compatible with the observed γ-ray flux.

5. CONCLUSIONS

HESS observations have led to the discovery of the shell-type SNR RCW 86 in VHE γ-rays. The γ-ray signal is significantly more extended than the HESS PSF. The possibility of a shell-like morphology was addressed, but cannot be settled on the basis of the limited statistics available at the moment. The flux from the remnant is $\sim$10% of that from the Crab nebula, with a photon index of about 2.5. The question of the nature of the particles producing the γ-ray signal observed by HESS is also discussed.

In a leptonic scenario, assuming that the γ-ray emission is entirely due to the IC process on cosmic microwave background photons and that the synchrotron and IC photons are produced by the same electrons, the ratio of the γ-ray energy flux and the X-ray flux determines the magnetic field to be close to 30 μG.

In the hadronic scenario, the lack of information about the low-energy γ-ray spectrum results in large uncertainties on the total energy budget in protons. If below several tens of TeV, the proton spectrum has a E^{-2} type spectrum, the total energy in protons would be in reasonable agreement with theoretical expectations. On the other hand, if we assume that the proton spectrum continues down to GeV energies with the observed spectral index $\Gamma = 2.4$, energetics would rule out a hadronic origin for the TeV γ-rays unless the SNR is nearby, or if the γ-rays are produced in a very dense medium as reported in the southern part of the remnant.

REFERENCES

Aharonian, F. 2001, A&A, 112, 307
Aharonian, F. (H.E.S.S. Collaboration) 2004, Astropart. Phys., 22, 109
Aharonian, F., et al. (H.E.S.S. Collaboration) 2005, A&A, 430, 865
Aharonian, F., et al. (H.E.S.S. Collaboration) 2006, A&A, 457, 899
Aharonian, F., et al. (H.E.S.S. Collaboration) 2007a, A&A, 464, 235
Aharonian, F., et al. (H.E.S.S. Collaboration) 2007b, A&A, 661, 236
Albert, J., et al. 2007, A&A, 474, 937
Bamba, A., Koyama, K., & Tomida, H. 2000, PASJ, 52, 1157

Bamba, A., Yamazaki, R., Yoshida, T., Terasawa, T., & Koyama, K. 2005, ApJ, 621, 793

Berge, D., Funk, S., & Hinton, J. 2007, A&A, 466, 1219

Berezhko, E. G., & Völk, H. J. 2006, A&A, 451, 981

Bernlöhr, K., et al. 2003, Astropart. Phys., 20, 111

Bocchino, F., Vink, J., Favata, F., Maggio, A., & Sciortino, S. 2000, A&A, 360, 671

Borkowski, K. J., Arnaud, K. A., Dorman, B., Hughes, J. P., Sarazin, C. L., & Smith, R. A. 2001, ApJ, 550, 334

Claas, J. J., Kaastra, J. S., Smith, A., Peacock, A., & de Korte, P. A. J. 1989, ApJ, 337, 399

Clark, D., & Stephenson, F. 1977, The Historical Supernovae (Oxford: Pergamon Press), 83

de Naurois, M. et al. 2005, in Proc. Conf. Towards a Network of Atmospheric Cherenkov Detectors VII, ed. B. Degrange & G. Fontaine (Palaiseau: Ecole Polytechnique), 173

Hinton, J. A. 2004, New Astron. Rev., 48, 331

Kelner, S. R., Aharonian, F. A., & Bugayov, V. V. 2006, Phys. Rev. D, 74, 3

Kesteven, M. J., & Caswell, J. L. 1987, A&A, 183, 118

Petre, R., Allen, G. E., & Hwang, U. 1999, Astron. Nachr., 320, 199

Pisarski, P. L., Helfand, D. J., & Kahn, S. M. 1984, ApJ, 277, 710

Porter, T. A., Moskalenko, I. V., & Strong, A. W. 2006, ApJ, 648, L29

Rho, J., Dyer, K. K., Borkowski, K. J., & Reynolds, S. P. 2002, ApJ, 581, 1116

Rosado, M., Ambrocio-Cruz, P., Le Coarer, E., & Marcelin, M. 1996, A&A, 315, 243

Smith, R. C. 1997, AJ, 114, 2664

Ueno, M., et al. 2007, PASJ, 59, 171

Vincent, P., et al. 2003, in Proc. 28th International Cosmic Ray Conference, ed. T. Kajita et al. (Tokyo: Universal Academy Press), 2887

Vink, J., Bleeker, J., Van Der Heyden, K., Bykov, A., Bamba, A., & Yamazaki, R. 2006, ApJ, 648, L33

Völk, H. J., Berezhko, E. G., & Ksenofontov, L. T. 2005, A&A, 433, 229

Watanabe, S., et al. (CANGAROO Collaboration) 2003, in Proc. 28th International Cosmic Ray Conference, IUPAP, ed. T. Kajita et al. (Tokyo: Universal Academy Press), 2397

Winkler, P. F., Jr. 1978, ApJ, 221, 220